Enhanced subsurface response for marine CSEM surveying

Frank A. Maaø and Anh Kiet Nguyen, EMGS ASA*

Summary

A new robust method for enhancing marine CSEM subsurface response is presented. The method is demonstrated to enhance resolution and depth penetration significantly.

Introduction

In the very early attempts to use marine controlled source electromagnetic (CSEM) measurements for hydrocarbon exploration, an application called seabed logging (SBL), it was considered to be a deep water exploration technology (Eidesmo et al. 2002). This was mainly caused by the reduced relative response from thin resistive layers in a shallow water environment.

However, these conclusions were based on examples where the deep water response was tenfold. Since then, it has become obvious that much smaller responses can be significant. Recent investigations reveal that sufficient subsurface response for detection of thin resistive layers is usually present also in shallow water environments. Mittet (2008) showed that anomalous responses could be seen in very shallow waters (40 meters), and Weiss (2007) concluded that transient measurements in 100 meters of water can detect targets at 2 km burial depth.

Several methods have been proposed to enhance the subsurface response in a shallow water environment. Among these are up-down separation (Amundsen et al. 2006), usage of azimuth data (Løseth and Amundsen 2007), and by applying spatial de-convolution methods (van den Berg et al. 2008). One often encountered challenge with methods aimed at enhanced subsurface response is the requirement to measurement accuracy. In order to extract information which constitute a small fraction of the total signal, the subtraction process must be done with a very high degree of accuracy. It is therefore important to find enhancement methods for the subsurface response that involves as little uncertainty as possible. We now present a new technique for enhancing the CSEM subsurface response which shows a particularly large potential in a shallow water environment and that involves a minimum degree of uncertainty.

Theory

The significance of any measured physical quantity, F^{obs}, can be accessed by comparing its deviation from some hypothetical value, F^{synth}, with its uncertainty, ΔF. This is often expressed in terms of an L2-norm misfit function

$$\varepsilon = \frac{\left|F^{obs} - F^{synth}\right|^2}{\alpha^2 \left|F\right|^2 + \left|n_F\right|^2}. \quad (1)$$

The uncertainty, ΔF, typically consists of two parts; one multiplicative, here represented with the term $\alpha\left|F\right|$, and one additive noise term, $\left|n_F\right|$. The multiplicative uncertainty typically arises from uncertainties in the acquisition parameters (positions, orientations etc.). The additive uncertainty is due to noise. Such noise can be caused by the instrumentation or any external uncontrolled signals. For marine electromagnetic measurements external noise sources can be due to natural radiation, swell and sea water currents. A typical requirement for having a significant deviation between the quantities F^{obs} and F^{synth} is $\varepsilon > 1$. A significant deviation between two scenarios then depends both on the sensitivity of F towards changes in the subsurface and of the measurement precision.

Often sensitivity can be enhanced by using derived quantities. However, derived quantities often involve an increase in uncertainty and this may reduce the overall benefit. Consider the electric field measured at two different frequencies but on the *same* channel and with the *same* source position and orientation. If we now consider a linear combination of these, the uncertainty of the linear combination will be proportional to the linear combination itself, plus the external noise of the original data (assuming the noise is uncorrelated with respect to frequency). Thus, if we define

$$F(\omega) = E(\omega + \Delta\omega) - E(\omega) \quad (2)$$

, the multiplicative uncertainty will be proportional to $F(\omega)$ and *not* $E(\omega)$. The electric field values, $E(\omega)$, are assumed to be normalized with source strength and phase (i.e. impulse responses). The quantity defined in equation (2) can show a high degree of subsurface sensitivity. For later reference these types of quantities will be referred to as *frequency differenced* data. The frequency differenced data can be also be interpreted in terms of the transient impulse response since

$$F(\omega) = E(\omega + \Delta\omega) - E(\omega) \simeq$$
$$\Delta\omega\, \partial_\omega E(\omega) = \Delta\omega \int_0^\infty dt\, it\, E(t) e^{i\omega t} \quad (3)$$

Thus, the frequency differenced data emphasize late-coming "events" in the signal. In the following we will

show some basic results from 3D modelling and a synthetic case study with inversion. Based on this we will discuss the potential for this method.

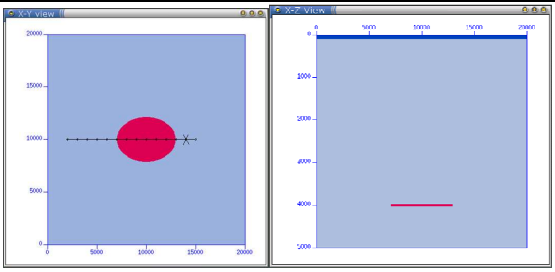

Figure 1: *A model used in the numerical example study consists of 100 meters of water, a homogenous background formation, and a 50 m thick resistive body. The conductivities are 3.2 S/m, 0.5 S/m, and 0.02 S/m respectively. The maximum length of the resistive body is 6 km, while the maximum width is 4 km. The burial depth of the resistive body is varied between 3 and 4 km. The left figure shows a horizontal cross-section at target depth and the black line indicates the synthetic survey layout with dots at receiver positions. The receiver position used for the numerical examples is marked with a cross. The right figure displays a vertical cross-section.*

Modeling example

Synthetic data was created using 3D modelling (Maaø 2007). The first set of models consist of 100 meters of water (3.2 S/m), a homogenous background formation (0.5 S/m), and a thin (50 m) resistive body with elliptic shape (0.02 S/m). The resistive body has semi axes of 6 and 4 km in the x- and y- direction respectively and its burial depth is varied. Figure 1 shows the model with the resistive body at 4 km burial depth.

To examine the sensitivity towards the presence of the resistive body, we normalize (divide) with data without the resistive body present. Figure 2 shows the normalized amplitudes and phases as a function of offset for the inline electric field and the frequency differenced data at some selected frequencies. Only very small changes in magnitudes and phases can be seen for the normal inline electric fields. Typically, the magnitude change is less than a few percent, while the phase change is less than a few degrees. The frequency differenced data shows a much larger sensitivity to the presence of the target. For Figure 2 the frequency difference used is 0.1 Hz. Clearly, the normalized magnitudes and phases show a much larger sensitivity towards the target. The sensitivity generally decreases when the frequency separation increases.

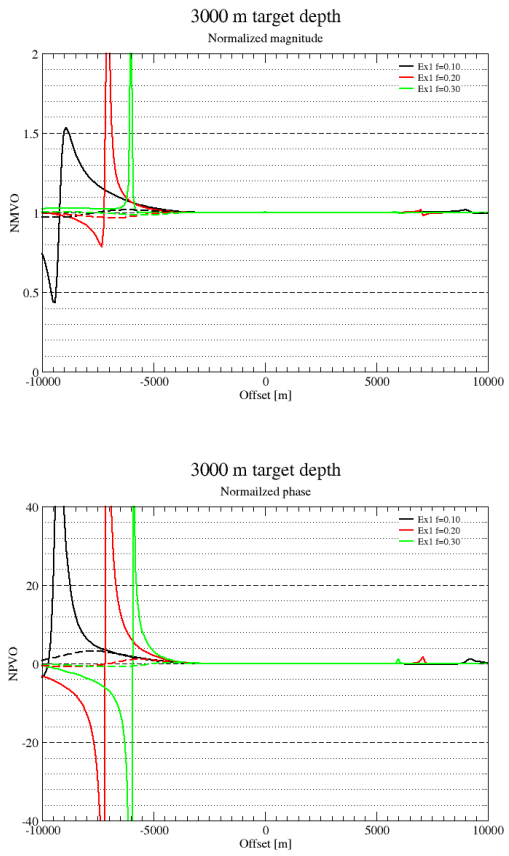

Figure 2: *The figures show normalized responses for a target depth of 3000 meters at 100 meters of water depth. Normalized magnitudes are shown on top while normalized phases are shown to the bottom (degrees). The responses of the frequency differenced data are shown in solid lines while the inline electric field responses are shown in dashed lines. The frequency separation used to produce the frequency differenced data is 0.1 Hz.*

The frequency differenced data show a great increase in sensitivity with respect to target sensitivity. However, the relevance of this sensitivity should be accessed through the misfit function, as defined in equation (1). For simplicity, the multiplicative uncertainty is set to 5% ($\alpha = 0.05$) of the inline data, and only the noise level, $|n_F|$, is varied. The square root of the misfit function is shown for various situations in Figure 3. We refer to this quantity as the *weighted sensitivity*. The effective noise levels used in these examples are 1.0×10^{-14} and 1.0×10^{-15} V / Am^2. While the normal inline data shows little response to the target

and is not much affected by the effective noise level, the frequency differenced data shows a much higher weighted sensitivity. This is particularly true for the smallest effective noise levels. At the very low noise levels the weighted sensitivities can be larger by more than an order of magnitude.

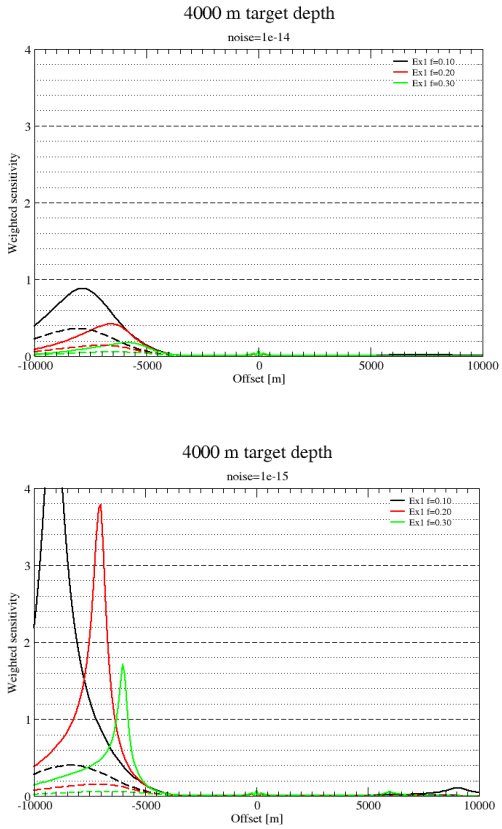

Figure 3: *The figure shows numerical results for weighted sensitivity for different noise levels and target depths as a function of source-receiver offset. The dashed lines refer to weighted sensitivities for the inline electric fields, while the solid lines refer to weighted sensitivities for the frequency differenced data. The difference in frequencies was set to 0.1 Hz.*

Inversion example

The misfit function defined in equation (1) was implemented in 2.5D inversion using both the conventional electric field *E* and the frequency differenced field defined in equation (3). Thus, two inversion schemes were implemented; one with a conventional misfit, and one where the misfit of frequency differences was added to the conventional misfit. We test the performance of the misfit functions using synthetic data from the 3D model shown in Figure 4. The model consists of a highly resistive basement (150 Ohm m) with large lateral variation in burial depth and large uplifts (two bodies) into the nearby overburden. The model also includes two layers of relatively high resistivity of 6 and 10 Ohm m just below the target. The target (100 Ohm) is a 100m thick and nearly elliptical shape at a 45 degree angle to the towline. It is approximately 2km wide, 4km long under the towline. The target depth is 3km and the resistivity of the overburden is 2 Ohm m. The water depth is 100m. The towline cross section of the model is shown in Figure 4. In the inversion, the four layers below the target and the water layer are inverted as areas of homogeneous resistivity while the rest of the model is inverted pixel by pixel. We use the background model, same model without the reservoir, as the starting model. Weak smoothness regularization is applied to stabilize the inversion. The frequencies selected where 0.1, 0.2 and 0.3 Hz with equal amplitudes. The effective noise floor was set to 1e-15 V/m for all frequencies.

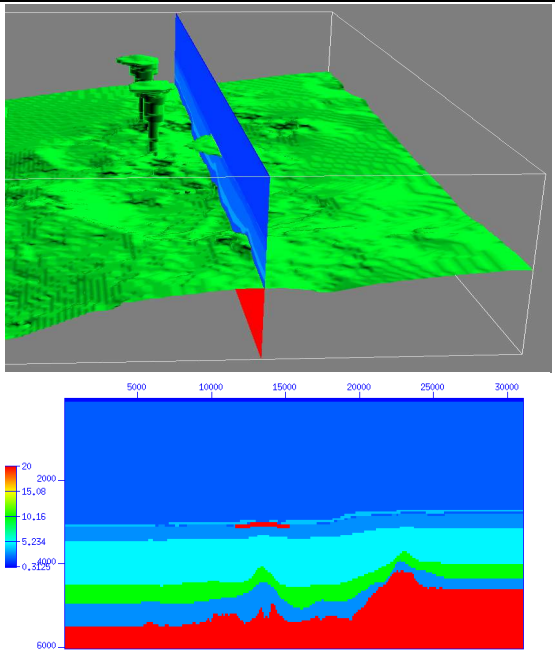

Figure 4: *Top: 3D model showing the high resitive (150 Ohm m) basement with uplifts, the reservoir and the towline. Bottom: 2D slice along the towline of the 3D resistivity model.*

Figure 5 shows the inverted models using the frequency differenced misfit and the conventional misfit. We see in Figure 5 that 2.5D inversion with the frequency differenced misfit puts in a resistivity anomaly at the correct depth. The anomaly was shifted slightly laterally due to the 3D shape of the reservoir that is not accounted for in a 2.5D inversion scheme. Thus, the horizontal position of the inverted resistive target is more in agreement with the center of the 3D target than with the position of the target at the given cross section. In contrast to this, 2.5D inversion using the conventional misfit is not able to find any resistivity anomaly. We also notice that the frequency differenced misfit function also provide much better resistivity of the constrained layers when comparing with the true model. In both cases, the average misfit for the inverted model are only 0.001, which corresponds to an average data error of 3%.

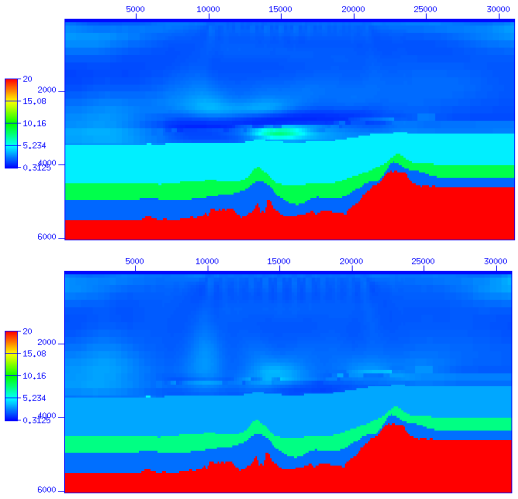

Figure 5: *Top: Inverted model after adding frequency differenced cost function to the conventional cost function. Bottom: Inverted model using conventional cost function.*

Discussion

In order to minimize uncertainty, the proposed method assumes data acquired on the same channel with signals emitted at the same source position and orientation. The latter can be obtained by emitting at two or more frequencies simultaneously. The only multiplicative uncertainty left, which is proportional to the original frequency dependent data, is therefore due the measurement of the source current and the calibration of the signal at the given frequencies. Note that any known systematic error in the frequency components can be compensated for and will not generate additional uncertainty. As shown in Mittet (2008), the scattered field caused by the presence thin resistive layers are usually larger in shallow waters than in deeper waters. Thus, aiming at methods to completely remove the sea surface interaction also means to reduce the magnitude of the scattered field. For sufficiently small or deep structures the scattered field may therefore end up below the effective noise floor. In the presented examples, the scattered field in the frequency differences has been of similar magnitude as for the scattered field of the single frequencies.

Conclusion

By utilizing frequency differencing we have found that a significant improvement in depth penetration and resolution can be achieved. This is particularly true in a shallow water environment. The method requires a sufficiently high signal to noise ratio.

Acknowledgements

We would like to thank EMGS for permission to publish the results and B. P. Thrane for help with Figure 3.

EDITED REFERENCES

Note: This reference list is a copy-edited version of the reference list submitted by the author. Reference lists for the 2009 SEG Technical Program Expanded Abstracts have been copy edited so that references provided with the online metadata for each paper will achieve a high degree of linking to cited sources that appear on the Web.

REFERENCES

Amundsen, L., L. Løseth, R. Mittet, S. Ellingsrud, and B. Ursin, 2006, Decomposition of electromagnetic fields into upgoing and downgoing components: Geophysics, **71**, no. 5, G211–G223.

Eidesmo, T., S. Ellingsrud, L. M. MacGregor, S. Constable, M. C. Sinha, S. Johansen, F. N. Kong, and H. Westerdahl, 2002, Sea bed logging (SBL) a new method for remote and direct identification of hydro carbon filled layers in deepwater areas: First Break, **20**, 144–152.

Løseth, L. O., and L. Amundsen, 2007, Removal of air-responses by weighting inline and broadside CSEM/SBL data: 77th Annual International Meeting, SEG, Expanded Abstracts, 529–533.

Maaø, F. A., 2007, Fast finite-difference time-domain modelling for marine subsurface electromagnetic problems: Geophysics, **72**, no. 2, A19–A23.

Mittet, R., 2008, Normalized amplitude ratios for frequency-domain CSEM in very shallow water: First Break, **26**, 47–54.

van den Berg, P. M., A. Abubakar, and T. M. Habashy, 2008, Removal of sea-surface wavefields and source replacement in CSEM data processing: 78th Annual International Meeting, SEG, Expanded Abstracts, 672–675.

Weiss, C., 2007, The fallacy of the “shallow-water problem” in marine CSEM exploration: Geophysics, **72**, no. 6, A93–A97.